

New method for the calculation of atomic phase shifts: Application to extended x-ray absorption fine structure (EXAFS) in molecules and crystals

P. A. Lee and G. Beni

Bell Laboratories, Murray Hill, New Jersey 07974

(Received 11 October 1976)

The scattering of electrons of kinetic energy up to 1000 eV by an atom is of special interest in the understanding of extended x-ray absorption fine-structure (EXAFS) spectra. An important physical feature is the reduction of the exchange and correlation potential as the kinetic energy of the electron increases. This is taken into account by replacing the atom by an electron gas with spatially varying density and calculating the self-energy using the plasmon pole approximation. This results in a set of complex phase shifts which is then applied to the EXAFS problem. Comparison is made with phase shifts extracted from experimental EXAFS spectra and excellent agreement is obtained. Direct comparison of the theoretical and experimental spectra again shows excellent agreement in both the amplitude and the phase. We also analyze the EXAFS spectra by a Fourier-transform technique which first removes the amplitude and phase shift using the calculated result. The importance of a proper choice of zero of energy E_0 is emphasized. We choose E_0 by the requirement that the imaginary part and the absolute value of the Fourier transform should peak at the same distance, thus assuring that the absolute phase is given correctly. Using this procedure the nearest-neighbor distances in Br_2 , GeCl_4 , and crystalline germanium are determined. In all cases the results are within 0.01 Å of the known distances. Several shells in germanium are also determined, with accuracy of better than 1%. Application of our method to crystalline copper indicates that the outer shells are more seriously affected by multiple-scattering problems and our procedure permits us to discard peaks that are spurious or unreliable. The present determination of the nearest-neighbor distance in copper is found to be in error by 0.014 Å. Results of the application of this method to the determination of the bond lengths of a variety of compounds are summarized.

I. INTRODUCTION

The phenomenon of extended x-ray absorption fine structure (EXAFS) refers to the oscillation of the x-ray absorption coefficient as a function of x-ray energy above threshold. It has long been recognized that the physical origin of this phenomenon is due to final-state interference, i.e., the final state is modified by the presence of the surrounding atoms.¹ Interest in EXAFS has been revived in the past several years due to two developments. Firstly, it was pointed out by Sayers, Stern, and Lytle² that EXAFS contains structural information which can be extracted using Fourier-transform techniques. It is clear that EXAFS can become a particularly useful structural tool in complex situations where x-ray diffraction is unavailable. Examples are biological molecules,³ solutions,⁴ amorphous materials,⁵ and catalysts.⁶ Recently a suggestion was made that EXAFS may be used to determine surface structure of adsorbed atoms.⁷ Secondly important experimental advances have been made with the availability of synchrotron radiation. The greatly increased intensity means that good quality spectra can be obtained in a matter of minutes.⁸ It is clear that interpretation of these data presents much greater problems than the collection of the data itself.

The single-electron theory of EXAFS has been

placed on very firm formal footing by several recent work.^{9,10} It has been argued that unlike low-energy-electron diffraction (LEED), multiple scattering is not a serious problem in most cases in EXAFS.⁹ The single-scattering theory of the EXAFS oscillations normalized to the background absorptions is given by

$$\chi(k) = - \sum_j \frac{N_j}{k r_j^2} \text{Im}[Z(k, r_j) e^{2ikr_j} e^{2i\delta_1'(k)}] \times e^{-2\pi r_j} e^{-2\sigma_j^2 k^2}, \quad (1.1)$$

for excitation of an s state in a system in which the orientation of the sample has been averaged over. Equation (1.1) describes the modification of the electron wave function at the origin due to scattering by N_j neighbor located at a distance r_j away. The backscattering is described by the factor $Z(k, r_j)$ which can be calculated in terms of scattering phase shifts and which in general depends on the distance r_j . However, explicit evaluation⁹ has shown that this dependence is relatively weak for moderate to high-electron momentum k and that it is possible to replace $Z(k, r_j)$ by the backscattering amplitude

$$f(\pi) \equiv A(k) e^{i\theta(k)} = \frac{1}{2ik} \sum_l (2l+1) (e^{2i\delta_l} - 1) (-1)^l, \quad (1.2)$$

which is equivalent to approximating the spherical nature of the outgoing wave by a plane wave. We shall make this approximation in the rest of the paper. Also included in Eq. (1.1) is the $l=1$ phase shift δ'_1 of the excited atom and factors γ and σ_j to account for inelastic losses and Debye-Waller smearing, respectively. Finally the photoelectron momentum k is measured with respect to some energy E_0

$$k = [2(\Omega - E_0)]^{1/2} \quad (1.3)$$

where Ω is the photon energy. [We shall use atomic unit (a.u.) throughout, $\hbar = e = m = 1$. The unit of length is 0.529 Å and the unit of energy is 2 Ry = 27.2 eV.]

It is clear that a knowledge of the k dependence of the phase functions δ'_1 and θ is essential before the EXAFS expression Eq. (1.1) can be inverted to provide information on the distances r_j . One approach to this problem is to perform a Fourier transform of the data after conversion to k space.² The peak in the Fourier transform occurs at a distance which is shifted from the correct distance by typically 0.2 to 0.3 Å. By performing the Fourier transform first on systems with known distances, these shifts can be measured and then used to predict distances in unknown systems. The weakness of the approach is that since the phase functions are not exactly linear, the shift will depend on the weighting of the data before Fourier transforming, the range in k space over which data are available, and possibly on Debye-Waller factors. Furthermore the shift depends on the choice of E_0 . Consequently while good results can be obtained in systems that are sufficiently similar, generally the accuracy that can be achieved by this technique is limited. A second approach to the problem that has been very successful for simple systems is the least-squares fitting method. By parametrizing the phase-shift function $2\delta'_1 + \theta$ by a linear and quadratic term, for instance, Citrin, Eisenberger, and Kincaid¹¹ have extracted the phase-shift functions by best fitting the data directly. Furthermore these authors have shown that the phase-shift functions extracted from the same atomic pairs in different chemical environments are in excellent agreement with each other and that phase shifts extracted from one system can be used to predict distances in another system with an accuracy of 0.01 to 0.02 Å. By working with a nonlinear phase-shift function Citrin *et al.* avoid many of the difficulties associated with the Fourier-transform technique. However, the experimentally extracted phase shifts still depend on the choice of E_0 , and the problem of a proper choice of E_0 when one is

going from systems in radically different environments (e.g., from metal to molecules) has to be faced.

It would clearly be desirable to be able to calculate the phase-shift functions. While the phase shifts can be determined empirically, it is possible only to determine the combinations $2\delta'_1 + \theta$ and not the two contributions separately. That means that a separate experiment is required for every atom pair. On the other hand $2\delta'_1(k)$ and $\theta(k)$ can be calculated separately and one needs only to add the appropriate pair to compare with experiments. It is the goal of the present work to perform *ab initio* calculations of these phase shifts and to compare them with experiments. Furthermore we address ourselves to the problem of the proper choice of E_0 . We also address the problem of data analysis and show that if the knowledge of the phase-shift function is properly utilized, the Fourier-transform technique can be used to extract distances with great accuracy even in complex systems.

There have been several earlier attempts at *ab initio* calculations of EXAFS spectra using Hartree-Fock or Hartree-Fock-Slater theory for the scattering phase shifts.⁸⁻¹⁰ These have met with only qualitative success. The most serious problem is that there appear to be systematic errors which make the determination of distances using these calculated phase shifts to be in error by as much as 0.1 Å out of 2.5 Å in the case of copper. The source of this difficulty has been recognized by Beni, Lee, and Platzman¹² as being caused by the inadequate treatment of correlation effects. In particular they considered the excitation of the d band in copper and showed that this leads to important corrections to the Hartree-Fock calculation in the direction of better agreement with experiments. The main ingredient of this theory is the construction of a complex potential which depends on the photoelectron energy. However, the construction of this potential is quite involved and some approximations in the numerical work had to be made. In the present paper we propose an alternate scheme of constructing this complex potential which has the advantage that it is relatively simple to use. The resulting phase shifts are tested in a variety of systems including simple molecules and crystals like copper and germanium. The problems that arise in trying to extract distances from the data using calculated phase shifts will be discussed in detail. It is hoped that this work will clear up any confusion that might exist concerning the Fourier-transform method and lead to a better understanding of the limits of accuracy of distances determined using EXAFS.

II. APPLICATION OF THE LOCAL-DENSITY APPROXIMATION TO PHASE-SHIFT CALCULATIONS

As noted earlier the electron-atom-scattering problem involves basically the construction of an effective scattering potential that adequately accounts for the exchange and correlation effects caused by the electrons in the atom. To construct this potential we use essentially a Thomas-Fermi approach, in the sense that we describe the atomic system solely in terms of its electronic density. The inclusion of exchange in the Thomas-Fermi theory is well known. A further generalization of Thomas-Fermi theory to include correlation effects in atoms has also been taken up by a number of workers,¹³ who proposed to add to the Thomas-Fermi energy a term representing the correlation energy as a function of density. The basic idea behind obtaining this term is to apply homogeneous electron-gas relations locally. The simplest way of doing this is to assume that each volume element of the atom responds to the total field acting on it as if it were part of an infinite homogeneous electron gas of the same density. This assumption has been used for example by Brandt and Lundqvist¹⁴ to obtain a universal atomic photoabsorption cross section over a wide frequency range. A more formal investigation of the propagation of a single-excited particle in an electron gas with slowly varying density has been made by Sham and Kohn¹⁵ following the earlier work of Hohenberg and Kohn¹⁶ on the ground-state properties of an inhomogeneous electron gas. The propagation of an electron from \vec{r} to \vec{r}' at an energy ω is described by the single-particle Green's function $G(\vec{r}, \vec{r}', \omega)$ which satisfies the Dyson equation

$$\begin{aligned} &(-\omega - \frac{1}{2}\nabla^2)G(\vec{r}, \vec{r}', \omega) \\ &+ \int d\vec{r}'' \Sigma(\vec{r}, \vec{r}'', \omega)G(\vec{r}'', \vec{r}', \omega) = -\delta(\vec{r} - \vec{r}'), \end{aligned} \quad (2.1)$$

where

$$\Sigma(\vec{r}, \vec{r}', \omega) = V_0(\vec{r})\delta(\vec{r} - \vec{r}') + M(\vec{r}, \vec{r}', \omega - V_0(\vec{r}_0))$$

and $V(\vec{r}_0)$ is the electrostatic potential at $\vec{r}_0 = \frac{1}{2}(\vec{r} + \vec{r}')$. Sham and Kohn¹⁵ and later Ma and Brueckner¹⁷ argued that the mass operator M depends only on the density $n(\vec{s})$ in the vicinity of \vec{r} and \vec{r}' in the sense that $|\vec{s} - \vec{r}| \sim \max(\lambda_F, \lambda_{TF})$ where λ_F and λ_{TF} are the Fermi wavelength and the Thomas-Fermi screening length, respectively. Unlike the case of the ground-state energy, this argument is not rigorous and is based on the physically reasonable assumption¹³ that elementary excitations which the electron couples to can be defined locally and are relatively independent

of each other over a distance greater than the screening length. It then follows that if $n(\vec{r})$ is slowly varying on the scale of λ_F and λ_{TF} , the mass operator can be approximated as

$$M(\vec{r}, \vec{r}', \omega - V_0(\vec{r}_0)) \approx M_h(\vec{r} - \vec{r}', \omega - V_0(\vec{r}_0), n(\vec{r}_0)), \quad (2.2)$$

where M_h is the mass operator of a uniform electron gas of density $n(\vec{r}_0)$. The Green's function can be written in terms of eigenstates

$$G(\vec{r}, \vec{r}', \omega) = \sum_n \frac{\chi_n(\vec{r}, \omega)\chi_n^\dagger(\vec{r}', \omega)}{\omega - E_n(\omega)}, \quad (2.3)$$

which satisfy the equation

$$\begin{aligned} &[-E_n(\omega) - \frac{1}{2}\nabla^2 + V_0(\vec{r})]\chi(\vec{r}, \omega) \\ &+ \int d\vec{r}'' M_h(\vec{r} - \vec{r}'', \omega - V_0(\vec{r}_0); n(\vec{r}_0))\chi(\vec{r}'', \omega) = 0. \end{aligned} \quad (2.4)$$

Furthermore if the electron density is slowly varying on the scale of the local de Broglie wavelength of the electron in question (which is generally shorter than λ_F and therefore represents a less severe condition than that already assumed) one can go to a momentum representation of $M_h(\vec{r} - \vec{r}')$ locally. The local momentum of the electron is given by

$$\frac{1}{2}p(\vec{r})^2 + M_h(p, \omega - V_0(\vec{r}_0); n) = \omega - V_0(\vec{r}_0) \quad (2.5)$$

and we can approximate Eq. (2.4) by a Schrödinger-like equation

$$[-E_n(\omega) - \frac{1}{2}\nabla^2 + V_0(\vec{r}) + U(\vec{r}, \omega)]\chi(\vec{r}, \omega) = 0, \quad (2.6)$$

where the effective potential is given by

$$U(\vec{r}, \omega) = M_h(p(\vec{r}), \omega - V_0(\vec{r}); n(\vec{r})). \quad (2.7)$$

It is worth noting that for an excitation at the Fermi level $\omega = \mu$, $p(\vec{r}) = k_F(\vec{r})$ and from Eq. (2.5):

$$U(\vec{r}, \mu) = \mu - V_0(\vec{r}) - \frac{1}{2}k_F^2 = \mu_{xc}(n), \quad (2.8)$$

where $\mu_{xc}(n)$ is the exchange and correlation correction to the chemical potential. If only exchange is included, $U(\vec{r}, \mu) = -k_F/\pi$ is the well-known $\frac{2}{3}$ times the Slater $\rho^{1/3}$ approximation.

The above is a summary of the discussion by Sham and Kohn. We now make the applications to the electron-atom-scattering problem and follow the prescription given by Eqs. (2.5)–(2.7) to construct the effective potential $U(\vec{r}, \omega)$. For an atom the condition that the electron density be slowly varying in comparison with λ_F or λ_{TF} is at best marginal. But numerous work has indicated that the ground-state properties are well reproduced by the Kohn-Sham approximation.¹⁸ Furthermore near the Fermi level the use of Eq. (2.8) as a basis for treating exchange and correla-

tion in band-structure calculations has been well documented.¹⁹ In the present work we extend the use of the effective potential to higher electron energy. It is clear that if the effective potential works for electrons near the Fermi surface, it should work even better for more energetic electrons as the de Broglie wavelength gets shorter.

To implement Eqs. (2.5)–(2.7) for numerical calculations one needs to make further approximations. First we compute the self-energy in the plasmon pole approximation of Lundqvist^{19,20} which replaces the elementary excitations of an electron gas by a single pole. These authors have shown that the real part of the self-energy can be written as a sum of two terms, the screened exchange and the Coulomb hole terms,

$$\begin{aligned} \text{Re}\Sigma(\vec{k}, \omega) = & - \int \frac{d\vec{q}}{(2\pi)^3} \frac{4\pi e^2}{q^2} \frac{f(\vec{k}+\vec{q})}{\epsilon(q, \frac{1}{2}(\vec{k}+\vec{q})^2 - \omega)} \\ & - \omega_p^2 \int \frac{d\vec{q}}{(2\pi)^3} \frac{4\pi e^2}{q^2} \frac{1}{2\omega_1(q)} \\ & \times \frac{1}{\omega_1(q) - \omega + \frac{1}{2}(\vec{k}+\vec{q})^2}, \end{aligned} \quad (2.9)$$

where

$$\epsilon(q, \omega)^{-1} = 1 + \omega_p^2 / [\omega^2 - \omega_1^2(q)], \quad (2.10)$$

$$\omega_1^2(q) = \omega_p^2 + \epsilon_F^2 \left[\frac{4}{3} (q/k_F)^2 + (q/k_F)^4 \right]. \quad (2.11)$$

Here $f(\vec{k})$ is the Fermi distribution function and ω_p is the plasma frequency. The q dependence of $\omega_1(q)$ has been adjusted so that the Thomas-Fermi screening length is correctly reproduced in the static small q limit while $\omega_1(q)$ approaches the free particle limit $\frac{1}{2}q^2$ for large q . The imaginary part of Σ is given by

$$\begin{aligned} \text{Im}\Sigma(k, \omega) = & \frac{\pi \omega_p^2}{2} \int \frac{d\vec{q}}{(2\pi)^3} \frac{4\pi e^2}{q^2 \omega_1(q)} \\ & \times \{ f(\vec{k}+\vec{q}) \delta(\frac{1}{2}(\vec{k}+\vec{q})^2 - \omega_1(q) - \omega) \\ & + [1 - f(\vec{k}+\vec{q})] \delta(\frac{1}{2}(\vec{k}+\vec{q})^2 + \omega_1(q) - \omega) \} \end{aligned} \quad (2.12)$$

and corresponds to emission and absorption of plasmons. The accuracy of the plasmon pole approximation in reproducing random-phase-approximation results has been well documented and will not be reviewed here.¹⁹⁻²¹

Next we have to obtain the local momentum from Eq. (2.5). While the electrostatic potential $V_0(\vec{r})$ can be obtained by solving Poisson's equation using electron densities obtained from tabulated atomic wave functions, these are not obtained as self-consistent solutions of an inhomogeneous electron gas. Thus the direct use of $V_0(\vec{r})$ in Eq. (2.5) causes difficulty. For instance it may happen that $p(\vec{r})$ may become less than $k_F(\vec{r})$. To avoid

this difficulty we note that if the atom is treated as an inhomogeneous electron gas, the electrochemical potential μ must be independent of \vec{r} . Thus we can write

$$\mu = V_0(\vec{r}) + \frac{1}{2}k_F^2(\vec{r}) + \mu_{xc}(n(\vec{r})). \quad (2.13)$$

Using Eqs. (2.5) and (2.8) we obtain

$$\frac{1}{2}p^2(r) = \omega - \mu + \frac{1}{2}k_F^2 + U(\vec{r}, \mu) - U(\vec{r}, \omega). \quad (2.14)$$

Noting that U is a relatively small correction to the Fermi energy we shall simply approximate

$$\frac{1}{2}p^2(r) = \frac{1}{2}k^2 + \frac{1}{2}k_F^2, \quad (2.15)$$

where k is the momentum of the electron outside the atom, i.e., $\omega - \mu = \frac{1}{2}k^2$. Equation (2.15) represents the Thomas-Fermi description of an atom. Similarly we replace the frequency argument in Eq. (2.7),

$$\omega - V_0(\vec{r}) = \frac{1}{2}p^2(\vec{r}) + U(\vec{r})$$

simply by $\frac{1}{2}p^2(\vec{r})$ and avoid solving the self-consistency equation. Both of these approximations should introduce only negligible errors as $U(r) \ll \frac{1}{2}k_F^2(r)$ for the bulk of the atom.

To summarize our procedure is to first obtain the spatial dependence of the charge density $n(\vec{r})$ from Hartree-Fock wave functions. From this we obtain the local Fermi energy and the local momentum using Eq. (2.15). Then a complex potential is constructed which depends on the kinetic energy of the incoming electron

$$U(r, \frac{1}{2}k^2) = \Sigma(p(r), \frac{1}{2}p^2(r)) \quad (2.16)$$

and Σ is obtained numerically from Eqs. (2.9) and (2.12). This complex potential is added to the electrostatic potential $V_0(\vec{r})$ and the complex phase shifts calculated.

In Fig. 1 we show examples of the real and imaginary parts of $rU(\vec{r})$ for a bromine atom as a function of incident electron momentum k . The important feature is the expected switching off of the real part of the exchange and correlation potential as k increases. Furthermore for a given k , as we go deeper inside the atom, $p(r) \approx k_F$ and the full exchange and correlation potential is maintained. For comparison we have also plotted the $X\alpha$ potential $\alpha \frac{1}{2}k_F(\vec{r})/\pi$ with a choice of $\alpha = 0.8$. We see that in the region of the valence electrons this potential is very close to our calculated potential for low-electron energy. Of course near the atomic core $r_s \ll 1$ and our calculated potential switches over to the purely exchange value of $-k_F/\pi$. We also remark that whereas significant cancellations occur between the two terms in Eq. (2.9) near the Fermi level, the screened exchange term turns off very rapidly with increasing k and the Coulomb hole term becomes dominant. In

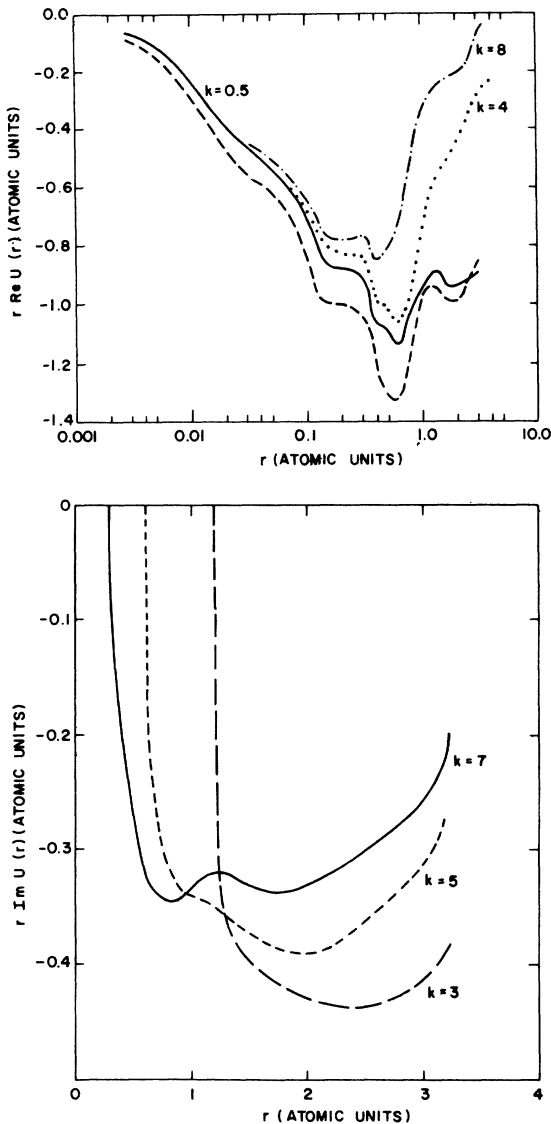


FIG. 1. (a) Plot of $r \text{Re} U(r)$ vs r on a logarithmic scale for a bromine atom with electron momentum $k = 0.5, 4,$ and 8 a.u. Dashed line is the $X\alpha$ approximation to $r \text{Re} U(r) = r\alpha(\frac{2}{3})k_F(\vec{r})/\pi$ with $\alpha = 0.8$. Note that for $r \geq 1$ this approximates the $k = 0.5$ curve whereas for $r \leq 0.1$ the Kohn-Sham value of $\alpha = \frac{2}{3}$ is a good approximation. (b) Plot of $r \text{Im} U(r)$ vs r for a bromine atom with $k = 3, 5,$ and 7 a.u. Atomic wave function has been truncated at $r = 3.24$ a.u. resulting in the discontinuity at this radius.

Fig. 1(b) the imaginary part of $U(\vec{r})$ is also plotted. The sharp cutoff at small r is due to the plasmon pole approximation which implies a definite threshold for inelastic processes that increases with decreasing radius and increasing Fermi energy. The inelastic process must correspond phys-

ically to excitations of various atomic bound states but a precise connection is not apparent within the inhomogeneous electron-gas treatment of the atom.

It is not possible to compare the real part of the potential U computed here with the complex effective potential of Beni *et al.*¹² This is because the exchange process is included in the former potential but not in the latter. However, we can compare the phase shifts calculated using the two schemes as we do in Fig. 2. The real part generally shows similar trends compared with the Hartree-Fock theory and is in good agreement with each other. The imaginary part is found to be smaller in the present scheme by about a factor of 3. This discrepancy is also apparent on comparing the imaginary part of the potential. Beni *et al.* have already discussed the possibility of overestimation due to approximations made in their computation. On the other hand, the excita-

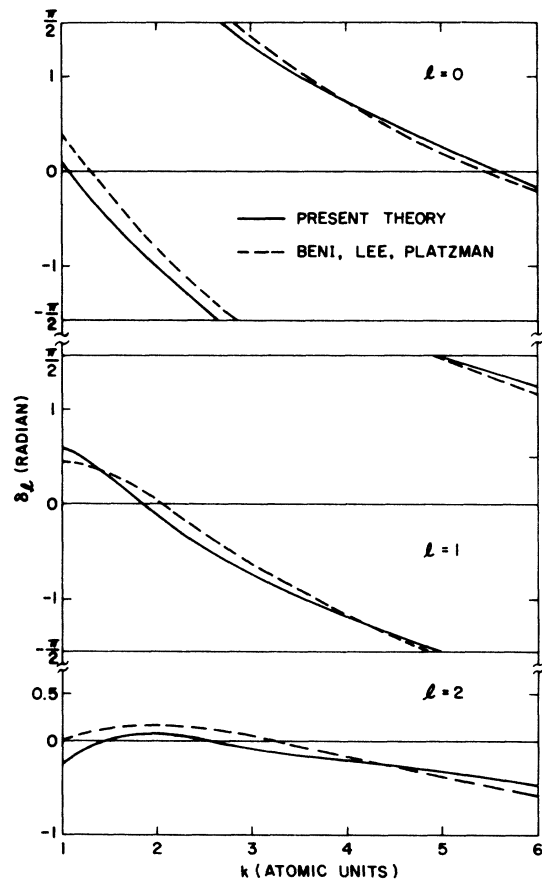


FIG. 2. Comparison of the present theory for δ_l with the calculation of Beni, Lee, and Platzman for copper. Wave functions have been truncated and renormalized inside the atomic radius for these calculations.

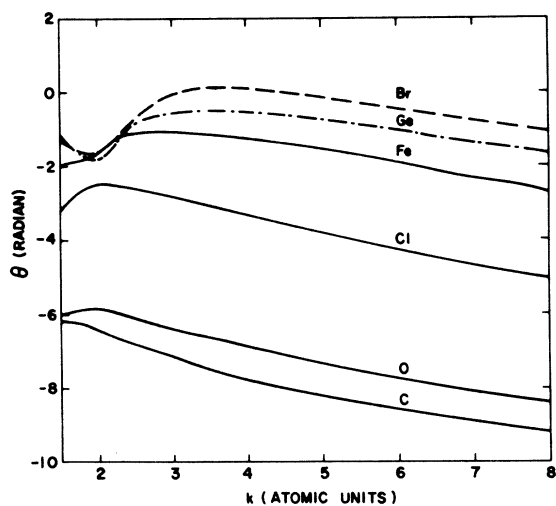


FIG. 3. Phase of the backscattering amplitude vs k for a number of atoms.

tion of bound d states is certainly more physically appealing than the excitation of local plasmons in an atom. The ultimate test of the reliability of the present scheme must lie in the comparison with experiments.

We have applied the above scheme to calculate a variety of electron atom phase shifts. Our main interests are the computation of the central atom phase shift $\delta'_l(k)$ and the backscattering amplitude $f(\pi) = A(k)e^{i\theta(k)}$. Figures 3 and 4 show the backscattering amplitude. The starting point is the Hartree-Fock wave functions tabulated by Clementi and Roetti.²² The wave functions are truncated at 1.5 times the atomic radius and a uniform charge density added to preserve charge neutrality within this radius. A complex effective potential is then constructed and the radial Schrödinger equation integrated up to the chosen radius to produce a set of complex phase shifts. For $l \geq 10$ we find that the phase shifts are generally small ~ 0.1 so that we may use first-order perturbation theory. This is particularly useful as direct integration becomes increasingly difficult numerically owing to the strong centrifugal potential. The perturbation method enables us to include 25 or more phase shifts which is the number required for convergence in $f(\pi)$ at $k = 8$ a.u. (870 eV).

The phase $\theta(k)$ is rather slowly varying as a function of k and changes systematically with increasing atomic number Z . The amplitude A generally peaks at low k for the lighter atom. When the electron exceeds the binding energy of the deepest shell, the electron is sampling mostly the nuclear potential and this explains the structureless tail for the lighter atoms like carbon and oxy-

gen. The heavier atoms like iron and germanium generally show a peak around $k \approx 4$, which moves toward higher k with increasing Z . This peak is associated with the $\frac{1}{2}\pi$ crossings of the $l=1$ and $l=2$ phase shifts as dictated by Levinson's theorem. The small k behavior ($k < 1.5$) is dominated by a strong d wave resonance in these cases and has not been shown. In this region a full multiple scattering theory (or band-structure calculation) is clearly required and is of no interest for the present purpose. The qualitative behavior of the amplitude shown in Fig. 4 generally agrees with the trends observed in EXAFS amplitudes. We also remark that $A(k)$ has a minimum near $k = 2$ for the heavy atoms like Fe or Br. When $A(k)$ is small, θ can be more rapidly varying and this is reflected in the downturn of $\theta(k)$ in the same region in k . This feature is insensitive to the details of the potential.

We have also calculated the $l=1$ phase shift for the central atom. The treatment of the central atom is considerably complicated by the presence of the $1s$ hole and the related question of relaxation of the surrounding electrons. In the Appendix we argue that the other electrons in the atom will relax inwards in response to the creation of the core hole and that the relaxed ion is well approximated by the $Z+1$ atom with an outer electron missing. We have calculated δ'_1 using the $Z+1$ atomic wave function and remove one outer shell electron. The Coulomb field is cut off at a radius chosen to be a typical bond length. We recognize that strictly speaking we should use a screened $Z+1$ atom (completely relaxed case) for low kinetic energy

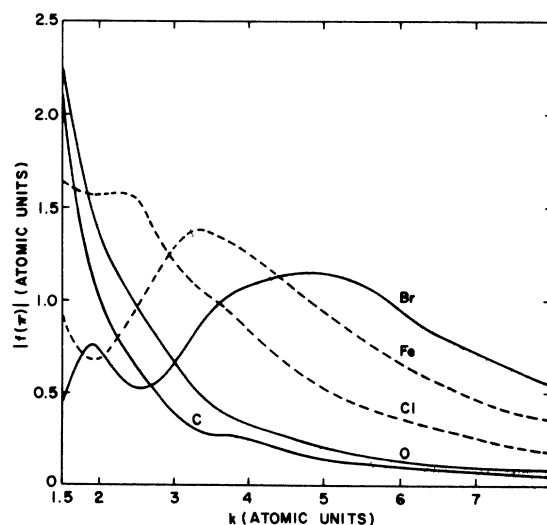


FIG. 4. Absolute value of the backscattering amplitude vs k for a number of atoms.

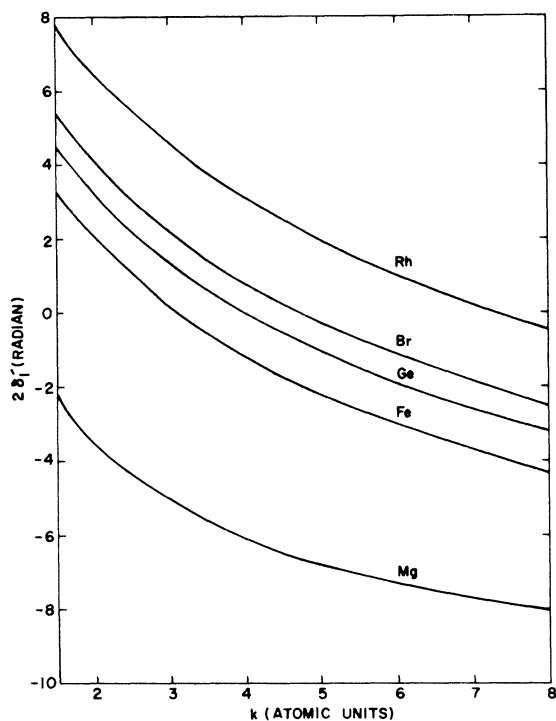


FIG. 5. Central atom phase shift $2\delta_1'$ vs k for a number of atoms.

and an unscreened Z ion (completely unrelaxed) for asymptotically high kinetic energy. The unscreened $Z + 1$ ion is chosen as a reasonable compromise. The difference between different extreme cases have been studied and roughly speaking can be compensated for by a change in the background potential E_0 by several eV. As we shall see in Sec. III there are other uncertainties in the choice of E_0 of the same order of magnitude.

Figure 5 shows the central atom phase shift for $l=1$ for a variety of atoms. We immediately see that it is a much stronger function of k and again vary systematically for increasing Z . In particular the potential is more attractive for increasing Z and we expect on general grounds that the phase shift should increase as is indeed the case.

III. APPLICATION TO EXAFS IN SIMPLE MOLECULES

Recently Citrin, Eisenberger, and Kincaid¹¹ have studied EXAFS from a number of simple molecules. Since a single distance is involved in these cases the EXAFS is approximately sinusoidal. By a least-squares fitting procedure these authors have been able to extract the phase shift

$$\phi = 2\delta_1' + \theta \quad (3.1)$$

as a function of k . A quadratic k dependence of

$\phi = ak^2 + bk + c$ was assumed for the fitting in the case of Br-Br, Ge-Ge, and Ge-C shown in Fig. 6. It has to be emphasized that these experimentally determined phase shifts are unique only if the choice of E_0 is specified. In particular it is obvious from Eqs. (1.1) and (1.3) that if E_0 is changed to $E_0' = E_0 + \Delta E_0$, then the momentum is redefined as

$$k' = (k^2 - 2\Delta E_0)^{1/2} \quad (3.2)$$

and the phase shift function is modified as

$$\phi'(k') = \phi(k) - 2r(k' - k) \approx \phi(k) + 2r\Delta E_0/k \quad (3.3)$$

for $2\Delta E_0 \ll k^2$. All quantities are in atomic units and r is the distance to the neighbor involved. As expected $\phi(k)$ is more sensitive to a change in E_0 at small k than at large k .

Citrin *et al.* chose E_0 to correspond to the vacuum level. This is in turn chosen by assuming that the sharp bound state observed in the absorption edge corresponds to the promotion of the 1s electron to the unfilled shell. In the case of bromine this must be the 4p shell and Kincaid and Eisenberger⁸ calculated this binding energy to be 13 eV.

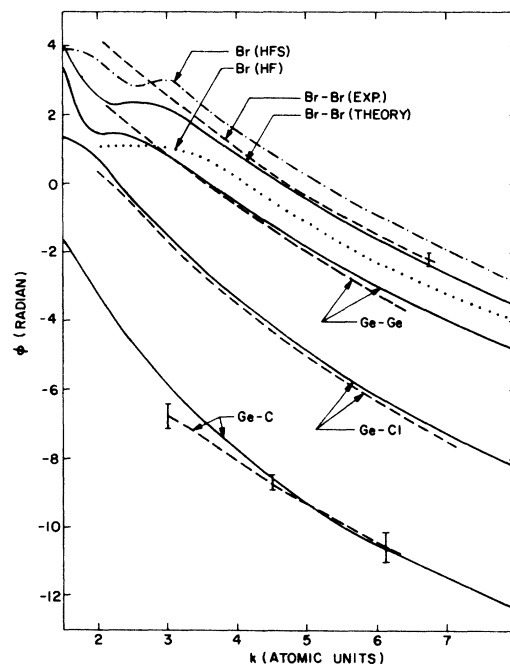


FIG. 6. Comparison of the total phase shift ϕ vs k for a number of atomic pairs, with Ge-C denoting Ge as a central atom and C the scatterer. For Br-Br the Hartree-Fock theory and the Hartree-Fock-Slater theory are also shown. Experimental results for Br-Br, Ge-Ge, and Ge-C are from Ref. 11 and the Ge-Cl result is from the analysis of GeCl_4 by B. M. Kincaid (unpublished).

Hence E_0 is chosen as 13 eV above the bound state. Alternately one could observe that the binding energy is well approximated by the ionization potential of the $Z + 1$ atom, which yields 14 eV for Br.²³ This choice of E_0 obviously ignored any chemical bonding effect which is of the order of 2 or 3 eV.

In Fig. 5 we compare our calculated phase shifts with the experimentally determined ones for a number of molecules. By simply adding the central atom phase shift and backscattering phase shift we are in effect overlapping the muffin-tin potentials. In reality the potential experienced by the electron in between the two Br atoms in Br_2 is undoubtedly not muffin-tin like. It is our hope that by overlapping the muffin-tin potentials the attractive potential in between the atoms is sufficiently well represented and we are in error by not more than a few eV. There are four uncertainties that we have discussed so far: (i) approximation of the spherical wave by a plane wave, (ii) approximate treatment of the relaxation of the central atom, (iii) approximate treatment of the molecular potential, (iv) the determination of the vacuum level from the experimental data. All of the above lead to larger errors in the phase shift function ϕ at small k than at large k . We then expect that the calculated phase shifts should agree with the measured ones at large k . Furthermore it should be possible to remove most of the discrepancy at lower k by adjusting E_0 by several eV. From Fig. 6 it is apparent that the agreement is excellent over a wide range of k for all of the atom pairs. Part of the discrepancy in Br_2 at low k , where the theoretical phase shift shows the downturn discussed earlier, is probably due to the assumed quadratic form of the experimentally determined phase shift. In any event it is clear from Eq. (3.3) and the uncertainties concerning E_0 that discrepancies at small k are much less serious than those at large k . If we turn the problem around and use the calculated phase shift to determine the distances, an error of ± 0.02 radians at $k=5$ implies an error of ± 0.01 Å in the distance determination. It is therefore hopeful that if (i) only data at large k are used, or (ii) E_0 is allowed to be adjustable, that we should be able to determine distances to ± 0.01 Å.

In Fig. 6 we also show the theoretical phase shifts of Br_2 if we use the Hartree-Fock theory or the $\rho^{1/3}$ approximation for exchange and correlation. For the latter we have used the $U(r)$ computed at low energy ($E=0.5$ in this particular case) for all values of k . The Hartree-Fock theory is clearly in serious error. However, the error decreases with increasing k and it is apparent that a change of E_0 by 10 to 15 eV might bring the

Hartree-Fock theory in rough agreement with experiment. On the other hand, the $\rho^{1/3}$ approximation differs from the measured ϕ by roughly a constant shift. Therefore a k -dependent E_0 shift is required to bring this theory into agreement with experiment. This is indeed the case for LEED calculations, as we shall discuss in greater detail in Sec. IV. Incidentally, Br has a large number of loosely bound electrons ($3d, 4s, 4p$) and the energy dependence of exchange and correlation is particularly important in this case.

We next use the calculated amplitude and phase curves to obtain a fit to the data and also to extract the distances. Figure 7(a) shows the comparison of theory and experiment for Br_2 . A Debye-Waller factor $2\sigma^2=0.0144$ a.u.² has been used.⁸ Use of the complex phase shift already included inelastic losses in the neighboring atom and no additional damping factor γ has been used. We find that it is necessary to multiply the theory by a factor of 0.62 to fit the overall magnitude. This has two physical origins. The first is the relaxation of the core hole which implies that only a fraction of the photoelectrons has been excited elastically. In the Appendix we estimate this fraction to be 74%. Secondly, inelastic processes in the central atom give rise to a complex δ'_1 . The imaginary part of $\delta'_1=0.144, 0.133, 0.099, 0.084$ at $k=2, 4, 6, 8$, respectively. The average value of $\exp(-2\text{Im}\delta'_1)\approx 0.75$. We must recognize that these two inelastic effects involve the same final states, i.e., a photoelectron plus an excited atom or ion, and we must add the amplitudes and not simply add the probabilities. Indeed the 74% estimate for the core hole relaxation contribution is for asymptotically high-energy electrons, when $\text{Im}\delta'_1$ becomes negligibly small.

Next we would like to extract the Br-Br distance in Br_2 pretending that it is not known. One approach is to use r as an adjustable parameter and try to obtain a best fit with emphasis on the large k value where the theory should be most accurate and also insensitive to changes in E_0 . Already from the phase shift curves and the quality of the fit shown in Fig. 7(a), particularly for $k>5$, it is clear that we will get the correct distance to better than 0.01 Å using the formula $\Delta r = \Delta\phi/2k$. A more flexible method, however, is that of Fourier transform because that can in principle also handle systems with more than one distance. That method has been widely used by Sayers, Stern, and Lytle.² What these authors do is to Fourier transform the data multiplied by k or k^3 and pick out peaks in the absolute magnitude of the transform. The peak position is typically shifted from the true distance by -0.2 to -0.3 Å due to the average slope of the $\phi(k)$ curve. These shifts are

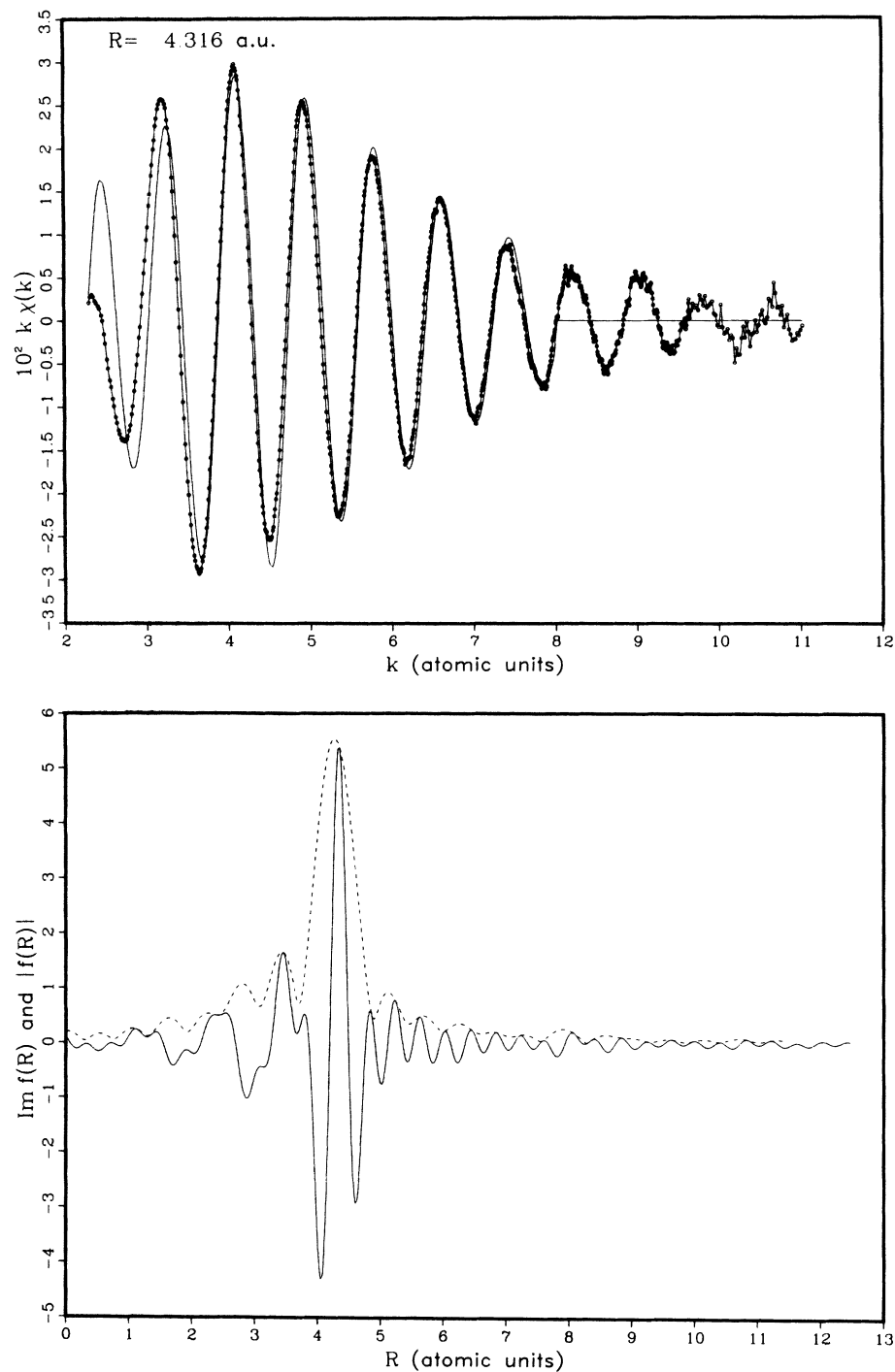


FIG. 7. (a) Comparison of theory (solid line) with the normalized experimental EXAFS spectrum (circles linked by solid line) for Br_2 . E_0 has been chosen to be 13 eV above the bound state. Theoretical curve stops at $k=8$. Theory curve has been reduced by a factor of 0.62 to fit the overall magnitude. (b) Fourier transform of the EXAFS data as defined by Eq. (3.4). Solid line is the imaginary part and dashed line the absolute value of the transform.

measured from studies of systems with known distances and applied to Fourier-transform unknown systems to extract the distances. One of the difficulties with this method is that the phase shift is not strictly linear. Thus depending on the weighting of the data the average slope of $\phi(k)$ can

vary. Furthermore, while the absolute value of the Fourier transform is insensitive to a constant shift in ϕ , it is sensitive to changes in E_0 , which affects $\phi(k)$ and therefore its average slope in the manner given in Eq. (3.3). Therefore uncertainties in E_0 become a serious limitation to the

accuracy that can be achieved. Now that we have a calculation of the phase shift curve it should be possible to eliminate these difficulties. Specifically we can remove the phase shift as well as the amplitude dependence on k before we Fourier transform, i.e.,

$$F(r) = \int \frac{dk e^{-i2kr}}{2\pi} e^{-i\phi(k)} \times \chi_{\text{expt}}(k) \frac{k}{A(k)} e^{2\sigma^2 k^2} g(k), \quad (3.4)$$

where $\chi_{\text{expt}}(k(E_0))$ is the experimental data with the background removed and $g(k)$ is a window function which selects out a range of the data. The window function can be a square window if care is taken to choose the cutoffs to be where χ_{expt} is small, or in our case we have chosen a smooth window,

$$g(k) = \begin{cases} \frac{1}{2}\{1 - \cos[\pi(k - k_1)/D]\}, & k_1 > k > k_1 + D, \\ 1, & k_1 + D > k > k_2 - D, \\ \frac{1}{2}\{1 + \cos[\pi(k - (k_2 - D))/D]\}, & k_2 - D > k > k_2, \\ 0, & \text{otherwise.} \end{cases} \quad (3.5)$$

We have chosen $k_1 = 2$ and $k_2 = 8$ for our range of analysis and $D = 0.05$. If χ_{expt} is well described by Eq. (1.1), it is easy to show that

$$\text{Im}F(r) \approx \frac{\sin 2k_2(r - r_1)}{r - r_1} - \frac{\sin 2k_1(r - r_1)}{r - r_1}, \quad (3.6)$$

for a square window function ranging from k_1 to k_2 . If $k_2 \gg k_1$ the first term dominates for r near r_1 and it is clear that $\text{Im}F(r)$ is a symmetric function peaked at $r = r_1$. Similarly

$$\text{Re}F(r) \approx \frac{-\cos 2k_2(r - r_1)}{r - r_1} + \frac{\cos 2k_1(r - r_1)}{r - r_1}, \quad (3.7)$$

which vanishes at $r = r_1$. The peak of $\text{Im}F(r)$ should coincide with the peak of the absolute value of the Fourier transform $|F(r)|$. This latter condition is a very sensitive check on whether the calculated phase shifts in fact fits the data well.

In Fig. 7(b) we show $\text{Im}F(r)$ together with $|F(r)|$. We see that $\text{Im}F(r)$ is fairly symmetric about its peak which is close to the peak in $|F(r)|$. The peak of $\text{Im}F(r)$ is located at 4.34 a.u. while the peak of $|F(r)|$ is about 4.27 a.u. Compared with the known distance of 4.316 ± 0.01 a.u. this is a rather satisfactory result.

Our next step is to recognize that the particular choice of E_0 to be 13 eV above the bound state is nothing sacred, and that this choice is itself subject to uncertainties of several eV due to the ne-

glect of the chemistry of the bonding. Furthermore we have already discussed that the theory contains uncertainties which are equivalent to uncertainties in E_0 . It is then natural to allow E_0 to be a free parameter and demand that the peaks of $\text{Im}F$ and $|F|$ coincide. This is done in Fig. 8. The fit achieved in Fig. 8(a) is excellent. The peak position of $\text{Im}F(r)$ is 4.310 a.u.

The very good agreement of the determined distance with the known distance is at first surprising. The following argument may help convince the rightfully skeptical reader that such accuracy indeed is possible. Let us suppose that there exist uncertainties in the calculated phase shift due to an error in the potential of 10 eV. The difference in phase due to this error can be estimated by making a change in E_0 of 10 eV which implies an uncertainty in $\phi(k=8)$ of only 0.2 radians using Eq. (3.3). Thus if we use only the data at $k=8$ to extract a distance, that distance is uncertain only to within $\Delta r = 0.2/2k = 0.012$ a.u. or 0.006 Å. Now the Fourier-transform is an average over all k values between 2 and 8 and it is evident from Fig. 5 that $\phi(k)$ does not have the accuracy of 0.2 radians over that range. However, by allowing E_0 to vary we can move $\phi(k)$ around according to Eq. (3.3) until a fit that is good to 0.02 radians on the average is obtained. The important point is by adjusting E_0 it is not possible to produce an artificially good fit with the wrong distance, provided that the phase shift is accurate for large k . This is because changes in E_0 produce a change in ϕ that *decreases* like $1/k$ according to Eq. (3.3) which is exactly opposite to a shift in distance which causes a change in ϕ that *increases* linearly with k .

Figures 9(a) and (b) show the same analysis of the GeCl_4 data allowing E_0 to vary. Electron diffraction measurements²³ have obtained a distance of 3.994 ± 0.006 a.u. as well as a Debye-Waller factor of $2\sigma^2 = 0.0145$ a.u.² In Fig. 9(a) this Debye-Waller factor and an overall factor of 0.43 have been used. The coincidence of the peak of $\text{Im}F$ and $|F|$ is achieved by the choice of E_0 to be 12 eV above the bound state. This is not too different from the 10 eV suggested by Kincaid *et al.*⁸ The peaks of $\text{Im}F$ and $|F|$ are at 3.981 and 3.990 a.u., respectively. Comparison with the distance determined by electron diffraction is again very satisfactory.

IV. APPLICATION TO EXAFS IN CRYSTALS

We next investigate the application of the calculated phase shifts to the analysis of EXAFS in two crystals: germanium and copper. Good qual-

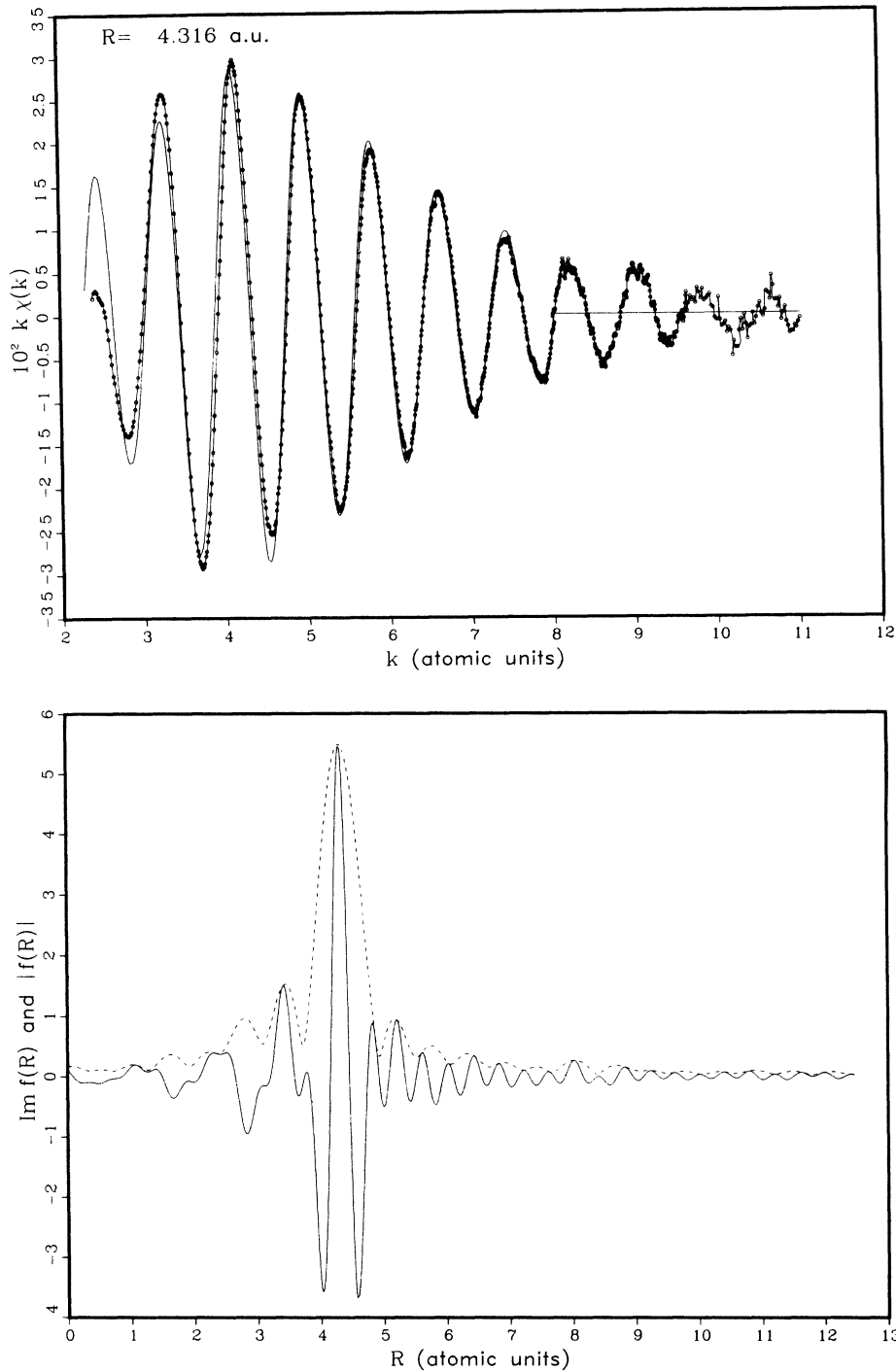


FIG. 8. (a)-(b) Same as Figs. 7(a) and (b) except that E_0 has been adjusted to make the imaginary part and the absolute value of the Fourier transform peak at the same radius. E_0 is found to be 7 eV above the bound state.

ity data taken at the synchrotron at Stanford at $\approx 100^\circ\text{K}$ for both systems have been made available to us. Germanium is a particularly favorable case as the diamond structure is relatively open so that multiple scattering effects are minimized. This is the case we shall examine first.

Figure 10(a) shows the theoretical spectrum generated using Eq. (1.1) and the amplitude and phase functions calculated as described earlier. The known nearest-neighbor distance 4.631 a.u. is used as an input. An imaginary self-energy $\Gamma = 6 \text{ eV}$ is assumed in between atomic sites, i.e.,

a damping factor of $\exp[-2\gamma(r_i - r_1)]$ is used, where $\gamma = \text{Im}(k^2 + 2i\Gamma)^{1/2} \approx \Gamma/k$ and the nearest-neighbor distance r_1 has been subtracted from the total traversed distance because damping by the scattering atom and the central atom has been included in the amplitude factor $A(k)$ and the

previously discussed overall factor which we now choose to be 0.7. A Debye-Waller factor of $2\sigma^2 = 0.022 \text{ a.u.}^2$ has been used for all the shells except the first shell, for which $2\sigma^2 = 0.011$ has been used. It is known that in a covalent material like germanium the nearest neighbor is directly bonded

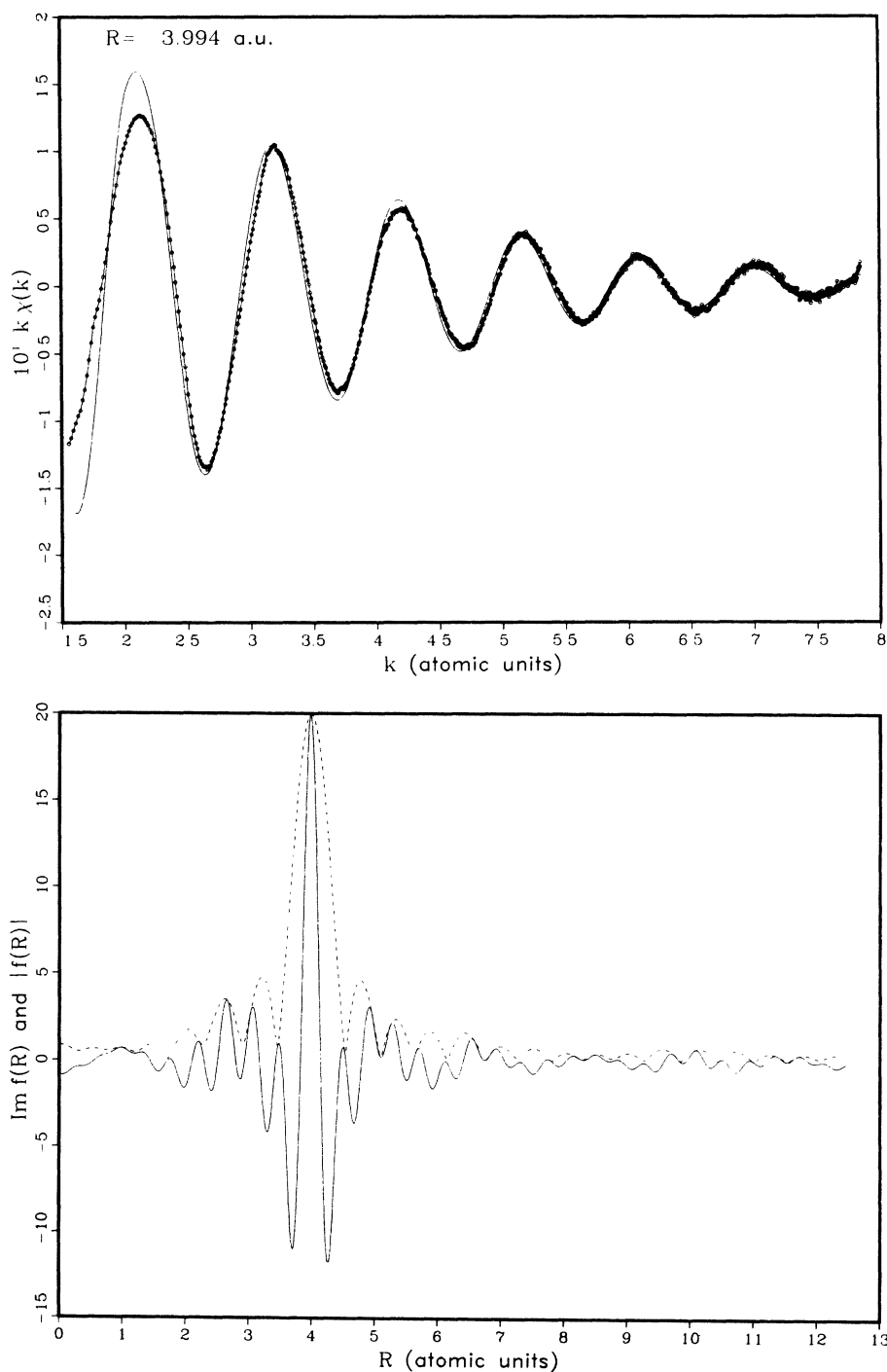


FIG. 9. (a)-(b) Comparison of theory and experiment for GeCl_4 . In Fig. 9(a) the theory has been reduced by a factor of 0.43 to fit the overall magnitude. E_0 has been chosen to be 12 eV above the bound state to make $\text{Im } F$ and $|F|$ match, as shown in Fig. 9(b).

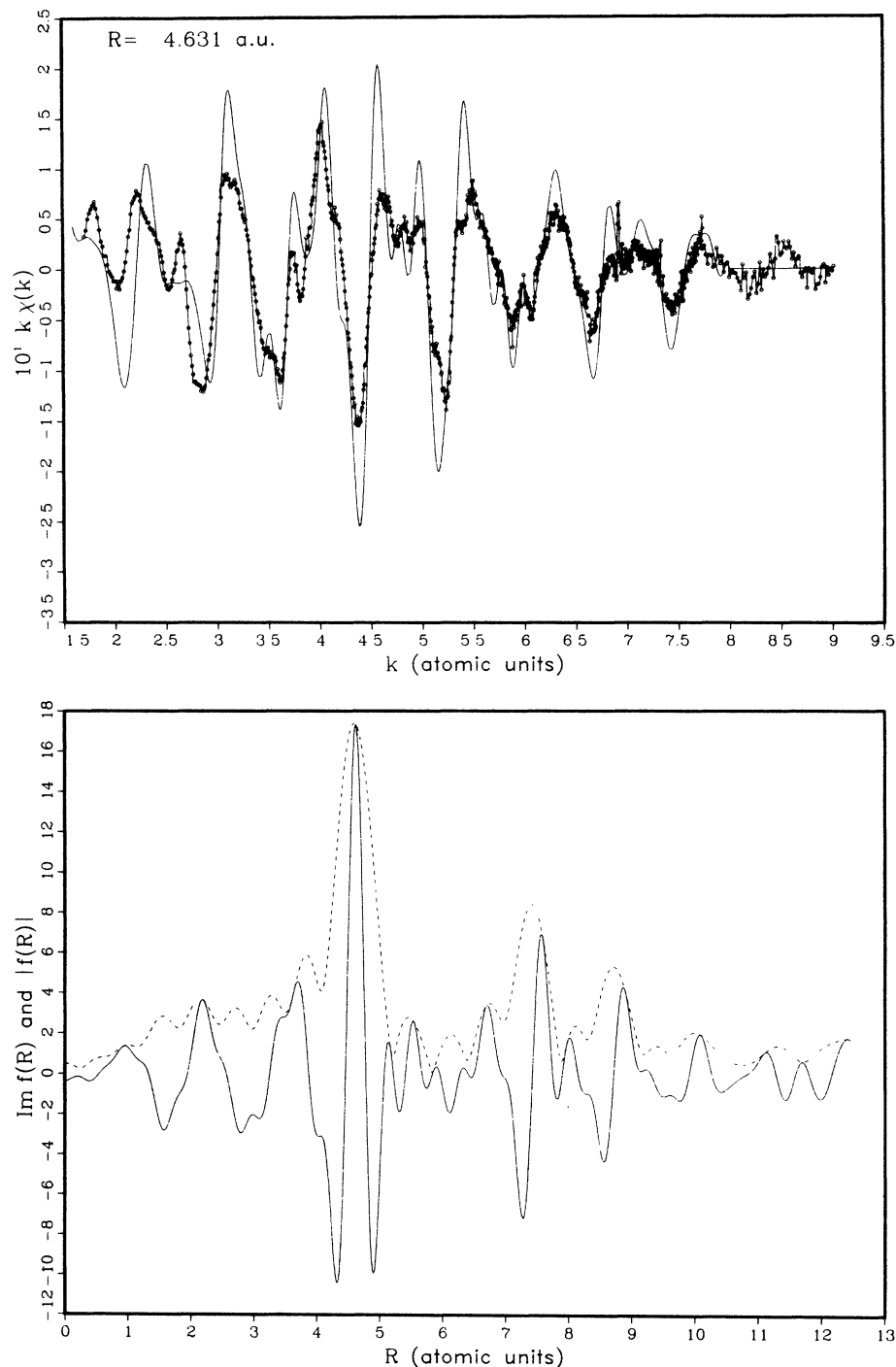


FIG. 10. (a)-(b) Comparison of experiment for germanium crystal (circles joined by solid line) with theory (solid line) calculated using $\phi = 2\delta'_1 + \theta$. E_0 is chosen to be 5 eV above the peak in the absorption edge to make $\text{Im}F$ and $|F|$ match for the first shell as shown in Fig. 10(b). Note that the other shells are out of phase.

resulting in strong correlation and a reduced Debye-Waller factor. Efforts to extract these shell-dependent Debye-Waller factors have been made by Sayers²⁴ by studying the temperature dependence of EXAFS. For our present purpose we simply chose these values of σ^2 because they give reasonable agreement with the data. No attempts

have been made to best fit the value of σ^2 or Γ and hence these parameters should not be viewed as determined.

In Fig. 10 E_0 has been varied until the $\text{Im}F$ and $|F|$ peaks for the first shell match up. The best E_0 is found to be 5 eV above the peak in the absorption edge. The distance corresponding to the

peak in $\text{Im}F$, for the first shell, is 4.619 a.u. which is in excellent agreement with the known distance of 4.631 a.u. However, it is immediately obvious that the other shells are in serious error. $\text{Im}F$ is completely out of phase and distances determined from the peak in $|F|$ are in error by almost 0.1 Å for the second and third shells.

The origin of this difficulty is immediately apparent. If we treat the crystalline potential by the nonoverlapping muffin-tin approximation (which is unacceptable for the accuracy demanded in band-structure calculations in Ge but is adequate for our purpose), the muffin-tin zero is below the vacuum level by more than 10 eV. For the nearest neighbor this attractive potential is taken into account by the overlapping muffin-tin approximation and by the freedom to change E_0 by a few eV. For neighbors further away this attractive potential is missing, and consequently additional phase shift needs to be taken into account.

We have overcome this difficulty by two different methods. The first obvious thing to do is to use the nonoverlapping muffin-tin zero as the zero of energy. The muffin-tin potential is constructed using the scheme of Mattheiss²⁵ in which one first performs a spherical average of the overlap between the electrostatic potential and also of the charge density. The effective potential $U(r)$ is then constructed within the nonoverlapping muffin-tin from the averaged charge density. The sum of this potential and the averaged electrostatic potential constitutes the nonoverlapping muffin-tin zero. A complex muffin-tin potential $V_{\text{MT}}(k)$ measured relative to the vacuum is obtained which is now energy dependent. (We have ignored the small discontinuity at the muffin-tin radius that exists if the potential due to the charge density in between muffin-tin spheres is properly taken into account.) The imaginary part is roughly 4 eV for copper over a wide energy range and slightly larger for germanium. This is consistent with conclusions drawn from analysis of LEED data. The real part is shown in Fig. 11 for germanium and copper. The muffin-tin potential extracted from analysis of LEED experiments²⁶ in Ni is also shown. The decrease of the magnitude of the muffin-tin potential with increasing energy agrees very well with the theory. It is known from band calculations that self-consistency calculations shift the muffin-tin zero upwards by about 3 eV (0.11 a.u.).²⁷ Thus even the absolute magnitude is in reasonable agreement.

The central atom phase shifts are recalculated using the energy-dependent muffin-tin potential as the zero of energy. We should use a nonoverlapping muffin-tin potential for the short-range part of the central atom potential as well. How-

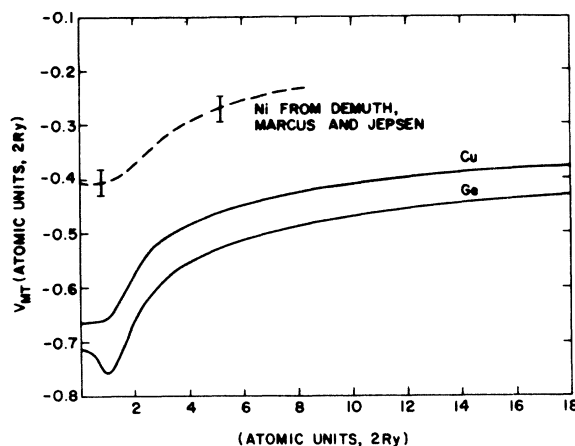


FIG. 11. The muffin-tin potential V_{MT} vs the electron kinetic energy for copper and germanium. Dashed line is from Ref. 27.

ever, we are content to use the atomic wave function as before which implies that some of the potential has been counted twice. We again correct for this by allowing E_0 to adjust.

The result of this calculation is shown in Figs. 12(a) and (b). The best choice of E_0 is found to be 2 eV above the peak at the absorption edge. The experimental spectrum is plotted in k' space where

$$k' = [k^2 - 2V_{\text{MT}}(k)]^{1/2} = \{\Omega - 2[E_0 + V_{\text{MT}}(k)]\}^{1/2}. \quad (4.1)$$

Again we perform a Fourier transform, this time in k' space by first multiplying that data by the calculated phase shift curve $\phi_{\text{MT}}(k')$. The result shows that except for the fourth shell, the peaks in the $\text{Im}F$ and $|F|$ are more properly aligned. The fourth shell is relatively weak since it contains only six atoms and it is probably distorted by some weak multiple-scattering features. The first shell of course remains within 0.01 Å of the known distance as before and the second and third shells are all accurate to within 1%. Except for the first shell, the difference of the peak position of $\text{Im}F$ and $|F|$ is a good indication of the extent to which a given distance determination is meaningful. This kind of information is essential if we are really going to apply EXAFS to unknown systems.

The muffin-tin method gives reasonable results, which can be further improved upon by using self-consistent potentials and a better central-atom potential. However, it has the disadvantage that a new phase-shift calculation has to be performed for each crystal structure. It would be much more desirable if the atomic phase shift functions, as shown in Figs. 3 and 5, can be used. This is the

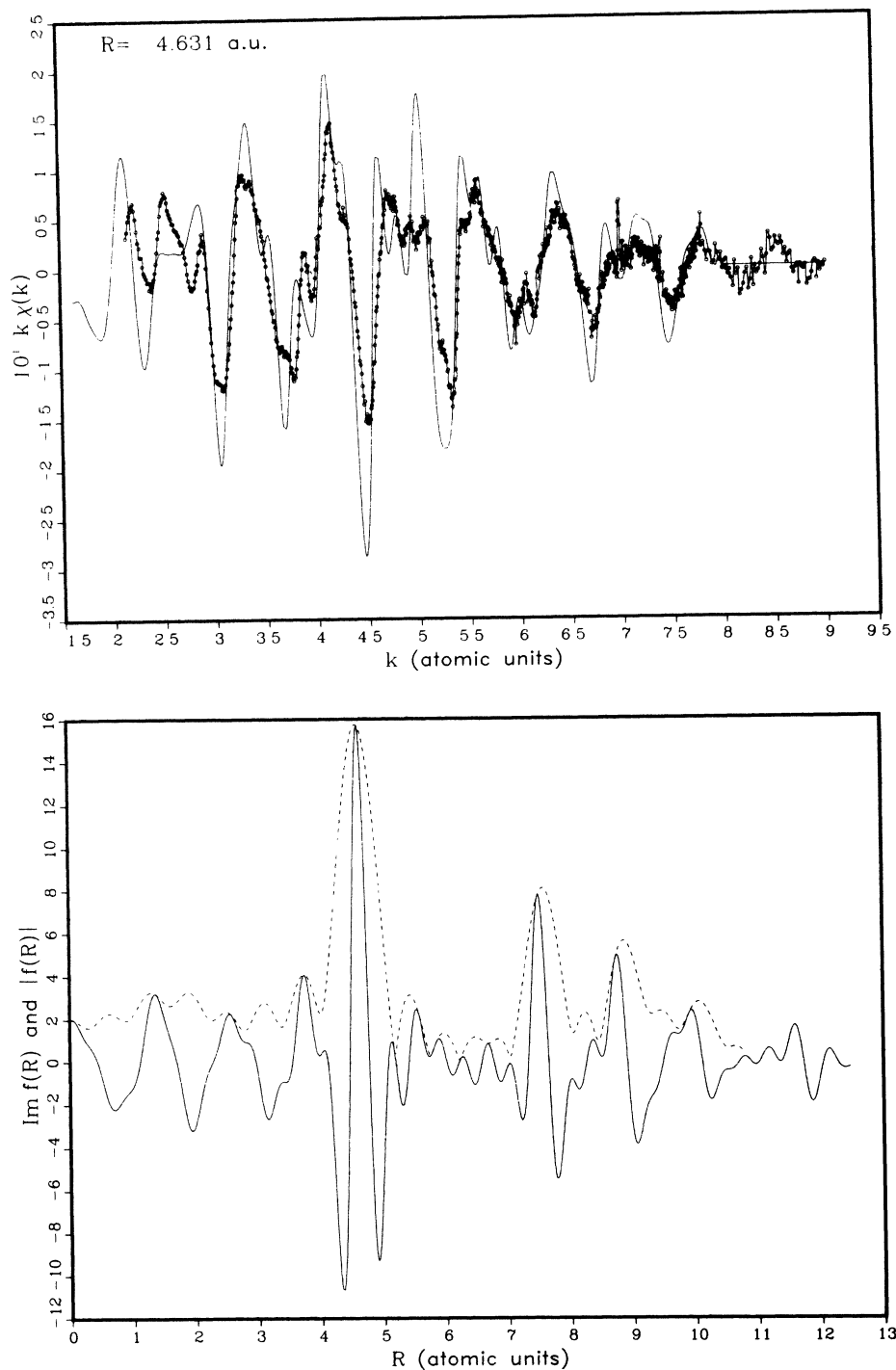


FIG. 12. (a) Comparison of the EXAFS spectrum for Ge with theory calculated using the non-overlapping muffin-tin potential. The X axis is k' is given by Eq. (4.1). (b) Shows the Fourier transform.

motivation behind the second method that we try. The idea is simply to construct a phase shift function $\tilde{\phi}$ from the function ϕ obtained from Fig. 3, which has the zero of energy not at the vacuum but at the muffin-tin zero. Furthermore since we know that the function $\phi(k)$ works for nearest

neighbors we shall demand that this property be preserved by the new phase shift function $\tilde{\phi}$. It is easy to see that $\tilde{\phi}$ is simply given by

$$\tilde{\phi}(k') = \phi(k) - 2r_1(k' - k), \quad (4.2)$$

when k' is given by Eq. (4.1). In Fig. 13, $\tilde{\phi}(k)$ is

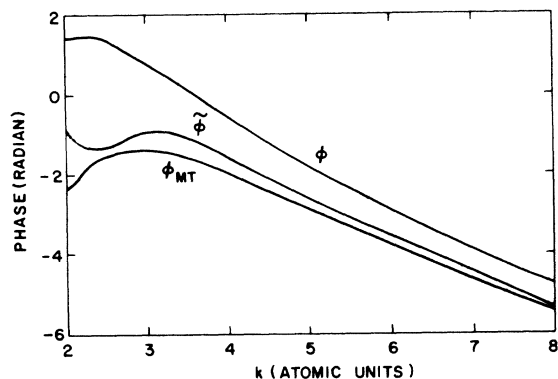


FIG. 13. Comparison of the phase shift functions ϕ , ϕ_{MT} , and $\tilde{\phi}$ for germanium.

compared with $\phi(k)$ and $\phi_{MT}(k)$. It is clear that $\tilde{\phi}(k)$ is very close to ϕ_{MT} . We now multiply $\chi_{\text{exp}}(k')$ by $e^{-i\tilde{\phi}(k)}$ as before and Fourier transform in k' space, again allowing E_0 to vary until the first shell has the proper phase behavior. The result is shown in Fig. 14 and is very satisfactory. The results of our analysis for germanium are summarized in Table I.

We next turn our attention to copper. Multiple scattering is a much more serious problem for a close-packed metal than for germanium, but as

we argued before,⁹ that should have no effect on the first shell. The most spectacular multiple-scattering effect shows up as the shadowing of the fourth shell by the first shell and this has been analyzed previously.^{9,12} The copper data shown in Fig. 15(a) are compared with the theory using the phase shift $\tilde{\phi}$ as discussed earlier and the parameters $2\sigma^2 = 0.022$ and $\Gamma = 6$ eV. The major features of the spectrum are reproduced by the agreement is poor compared with the case for germanium. The reasons are apparent from the Fourier transform shown in Fig. 15(b). The first shell is still satisfactory and peaks at 4.795 a.u. which is 0.025 a.u. shorter than the known distance.²⁸ The second shell in copper is weak and the phase distorted, probably by some multiple-scattering path. The third shell is in reasonable shape, with $\text{Im}F$ and $|F|$ peaking at 8.30 and 8.48 a.u., respectively. The difference between these two numbers indicates that our confidence level cannot be better than 0.2 a.u. in this case. This result is to be compared with the known distance of 8.35 a.u. The fifth shell is also within 1% of the known distance. The fourth shell shows the shadowing effect noted earlier, namely, its magnitude is larger than the third shell even though it contains 12 atoms, compared with the third shell's 24 atoms. Furthermore $\text{Im}F$ shows severe distortion. The exact amount of the phase shift is difficult to as-

TABLE I. Distances determined by Fourier transform of EXAFS.

System	E_0 (eV)	$ F $	$\text{Im}F$	Known distance (a.u.)
Br ₂	7 ^a	4.308	4.310	4.316 ± 0.01
GeCl ₄	12 ^a	3.990	3.981	3.994 ± 0.006
Ge				
1st shell ^c	2 ^b	4.605	4.626	4.631
1st shell ^d	7 ^b	4.632	4.628	
2nd shell ^c		7.574	7.499	7.563
2nd shell ^d		7.556	7.524	
3rd shell ^c		8.866	8.754	8.868
3rd shell ^d		8.869	8.785	
4th shell ^c		10.064 ^e	9.944 ^e	10.695
4th shell ^d		10.087 ^e	9.956 ^e	
5th shell ^c		11.762 ^e	11.593 ^e	11.655
5th shell ^d		11.601	11.635	
Cu				
1st shell ^d	3 ^b	4.794	4.795	4.820
2nd shell ^d		7.077 ^e	... ^e	6.817
3rd shell ^d		8.477	8.303	8.349
4th shell ^d		9.452 ^e	... ^e	9.641
5th shell ^d		10.648	10.730	10.779

^a Measured from the bound state.

^b Measured from the peak at the absorption edge.

^c Phase shift determined using muffin-tin potential.

^d Phase shift $\tilde{\phi}$ using Eq. (4.2) is used.

^e Peak is too distorted to make this distance determination meaningful.

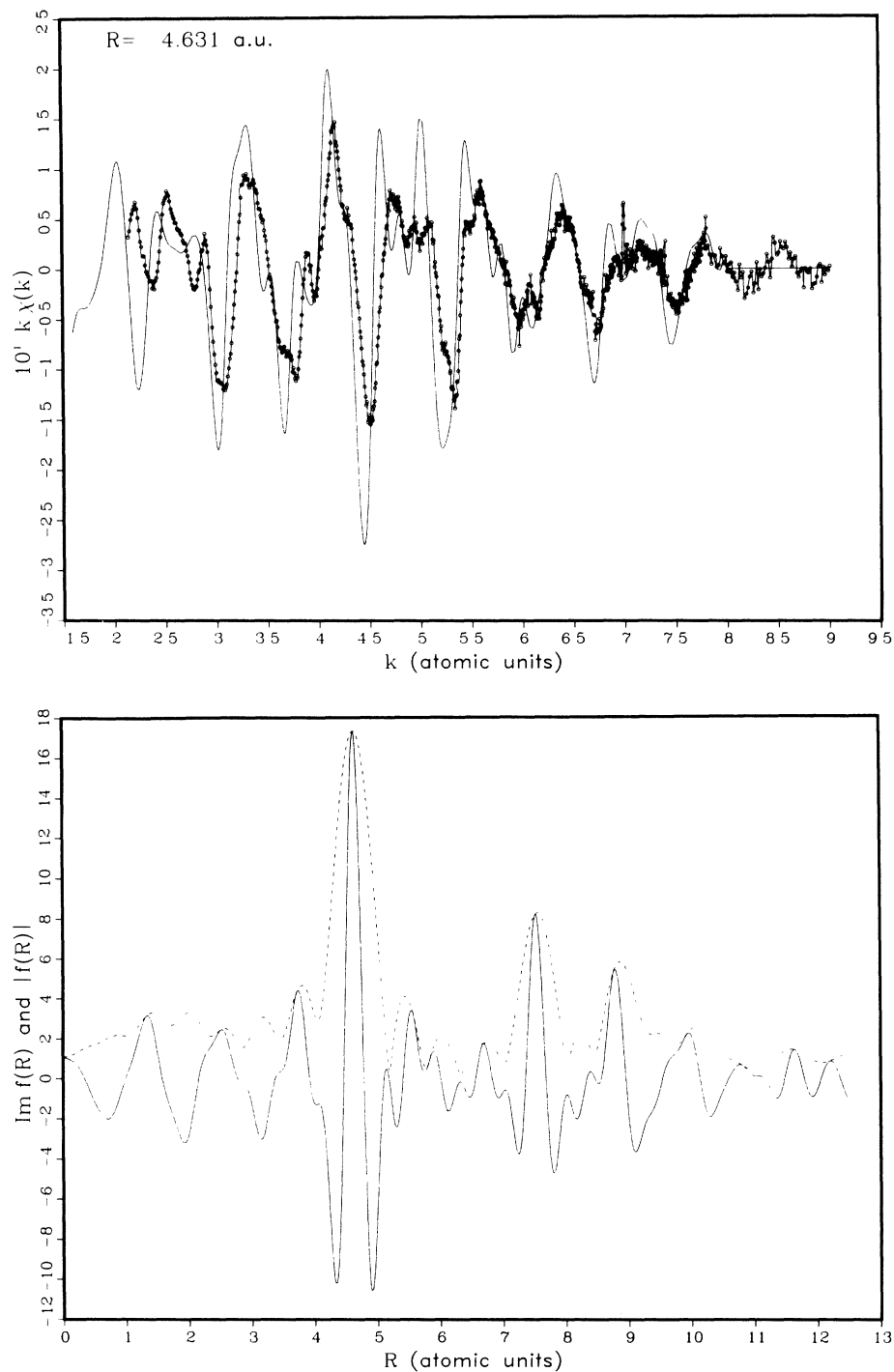


FIG. 14. (a) Comparison of the EXAFS spectrum for Ge with theory calculated using $\tilde{\phi}$ as given by Eq. (4.2). (b) Shows the Fourier transform.

certain and we can only state that the theoretical result¹² of an additional $\frac{1}{2}\pi$ phase shift is not inconsistent with the experimental result.

We have also performed a nonoverlapping muffin-tin calculation for copper. The result is not too different from that using $\tilde{\phi}$. It is amusing to note

that the real part of the phase shifts δ_l for the energy-dependent muffin-tin potential that we generate is quite close to the phase shift generated using an energy-independent $X\alpha$ -type muffin potential of the type used in LEED analysis. Apparently the use of an energy-dependent inner potential

determined empirically as shown in Fig. 11 takes care of a good deal of the switching off of the exchange and correlation potential at energies below 200 eV. This explains why LEED calculations are getting good agreement for metals. It will be of great interest to use the complex phase shifts

generated using the present scheme for LEED analysis, the advantages being (i) the energy dependence of the inner potential as well as the damping coefficient are calculated instead of being adjusted by hand, and (ii) even though the real part of the phase shifts is similar, the use of

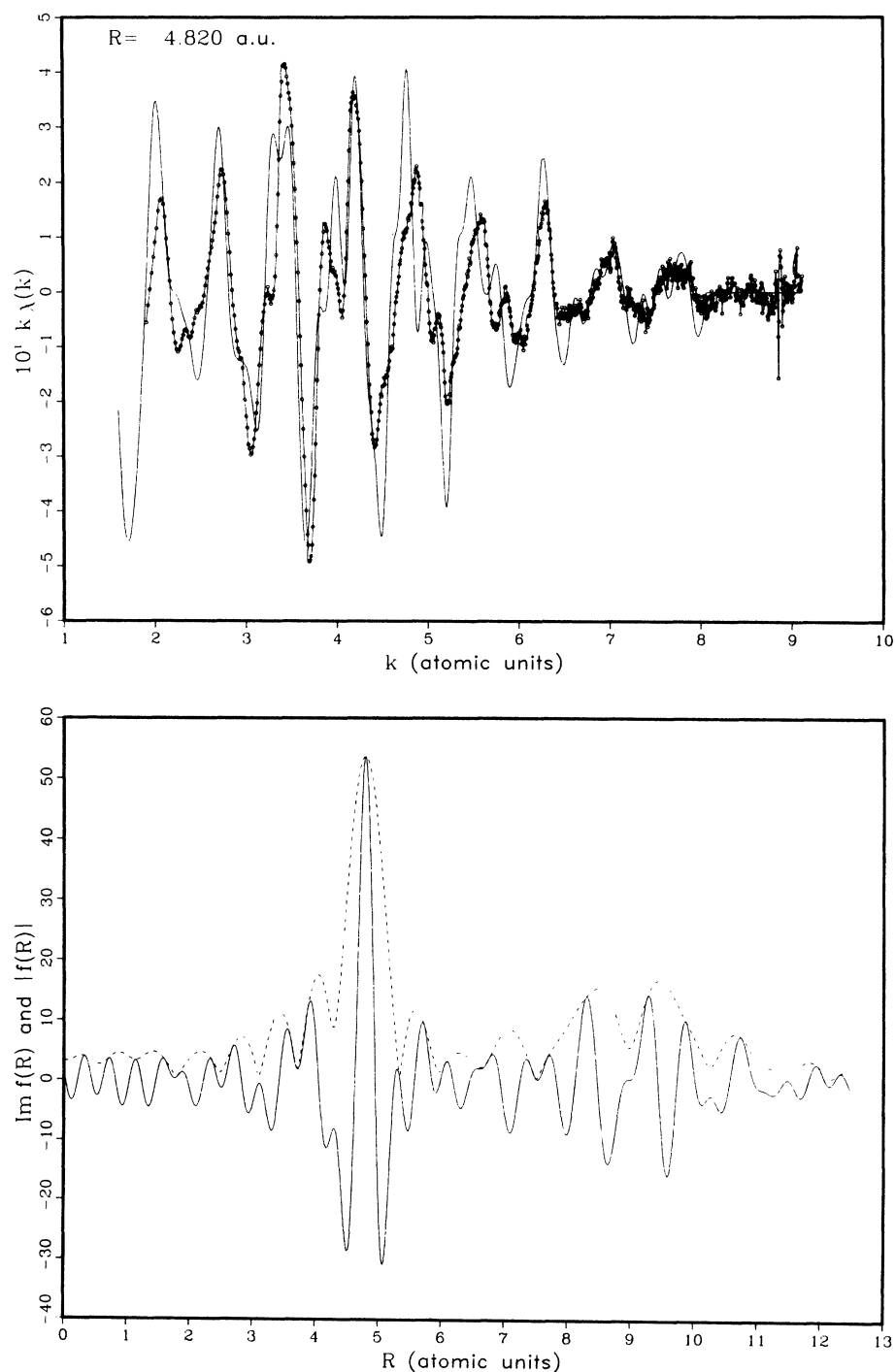


FIG. 15. (a) Comparison of the EXAFS spectrum for copper with theory using $\tilde{\phi}$ as given by Eq. (4.2). (b) Shows the Fourier transform.

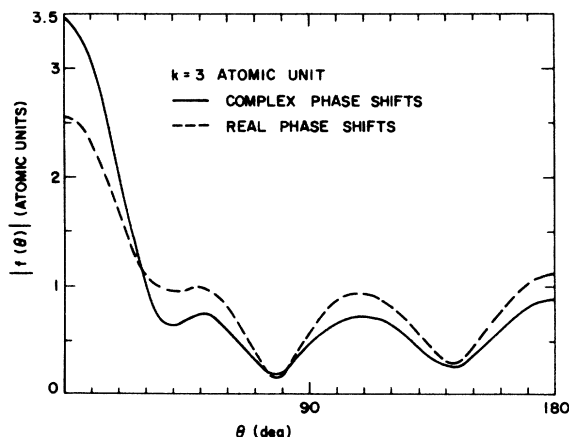


FIG. 16. The scattering amplitude $|f(\theta)|$ vs θ for the real and complex phase shift of an electron momentum of $k=3$ a.u.

complex phase shifts means that the scattering amplitude $f(\theta)$ can be quite different. In particular, in the forward direction $f(\theta)$ is enhanced by inelastic processes (a consequence of the optical theorem) whereas the use of real phase shift plus damping reduces $f(\theta)$ at all angles. This is illustrated in Fig. 16. Unlike EXAFS, which requires only $f(\pi)$, LEED will provide a test for the entire $f(\theta)$.

V. CONCLUSION

We have calculated the amplitude and phase shift that enters into the EXAFS expression using a relatively straightforward procedure which we feel contains the essential physics of the problem. These phase shifts are compared with those extracted from experiments and generally the agreement is as good as that among phase shifts of the same atom pairs extracted from experiments on different molecules. We also use these phase shifts to predict distances in both simple molecular systems and crystalline solids. We emphasize that the choice of E_0 is intimately related to the phase-shift curves. We then recommend a specific procedure whereby E_0 can be chosen and a distance determined. The results of the distance determination are summarized in Table I. We see that in all cases the nearest-neighbor distances are in excellent agreement. The worst discrepancy is 0.014 Å in the case of copper. For Ge multiple scattering is less important and we obtain distances to within 1% for four of the five shells. In copper multiple-scattering effects are much more serious and we can only obtain the distance to the third shell and the fifth shell with a confidence level of about 1%. An objection that

has often been raised concerning previous use of Fourier transform in the analysis of crystalline data is that the identification of a particular peak as a shell distance appears rather subjective. Our criterion that the peaks of $\text{Im}F$ and $|F|$ have to line up can be used to eliminate spurious peaks as well as provide information on the confidence level of a particular identification. It is with this criterion that we reject the second and fourth shell in copper and the fourth shell in germanium as being contaminated by background noise or multiple-scattering effects. Such information is not available if one studies only $|F(r)|$ as is done traditionally. We also emphasize that our method of distance determination relies on the knowledge of the absolute value of the phase $\phi(k)$ for large k and not on the average slope of the phase function, the latter being much more sensitive to uncertainties in the zero of energy E_0 .

It remains to discuss the errors that should be assigned to the distances determined. There are two sources of error. The first is the intrinsic accuracy of the calculated phase-shift functions themselves. We have argued that this error is partly offset by allowing E_0 to vary. Clearly the only way to assess this error is to compare with experiments on as large a variety of systems as possible. In Table II we summarize the results for all the systems we have studied to date using the present method. The data have been made available to us by our colleagues at Bell Laboratories and some of the data have not been published. We see that for scattering atoms that vary from carbon to bromine, the distance determination is in error by less than 0.02 Å in all cases. The second source of error is more accurately described as an assessment of the level confidence, i.e., given that the phase shift is accurate, what is the range of distances that gives a satisfactory fit to the experiment? This question we can answer for simple molecules as the quality of the fit shown in Figs. 8(a) and 9(a) allows us to state that a change in the distance by 0.01 Å will lead to inferior comparison with experiments. For the shells beyond the first one in crystals, we also have an indication in the difference in the peak position in $\text{Im}F$ and $|F|$. However, for more complicated systems like copper, for instance, the quality of the agreement in the experimental and theoretical spectrum shown in Fig. 15(a) is poor due to multiple-scattering effects. In this case we are unable to assign an error bar. More generally, in complex systems it is difficult to obtain a fit to the spectra without varying a large number of parameters such as the Debye-Waller factor, etc. This makes the assignment of error bars a difficult problem. Recently Brian Kincaid

TABLE II. Bond lengths determined by EXAFS.

Bond	Compound	Predicted (Å)	Known	Difference
Br-Br	Br ₂	2.279	2.283 ± 0.005	-0.004
Ge-Ge	Ge	2.449	2.450	-0.001
Cu-Cu	Cu	2.536	2.550	-0.014
Ge-Cl	GeCl ₄	2.108	2.113 ± 0.003	-0.005
Rh-Cl	RhCl ₃	2.337	?	
Fe-S	rubredoxin ^a model	2.343	2.356	-0.012
Rh-P	Rh(DPPE) ₂ ^b	2.288	2.305	-0.017
Br-O	BrO ₃ solution	1.66	?	
Ge-O	GeO ₂	1.727	1.739	-0.012
Fe-C	Fe(C ₅ H ₅) ₂	2.037	2.045	-0.008

^a Fe(S₂-o-xy1)₂²⁻.^b DPPE, diphenylphosphinoethane.

has used a Fourier-filtering technique to extract a phase-shift curve from isolated shells and has been able to assign error bars based on a least-squares fitting technique.

In summary, we have shown that the calculated phase shifts can be used to obtain distances to the same accuracy as the use of empirically determined phase shifts.¹¹ Use of theoretical phase shifts has the obvious advantage that the central atom part and the scattering part are calculated separately and can be put together in any combination, whereas empirical phase shifts must be determined separately for every atom pair. The intrinsic uncertainty is on the 0.01 Å level for nearest-neighbor-distance determination. Clearly we need to accumulate more experience in the analysis of more complicated systems, but it is our belief that the accurate determination of absolute distances in unknown systems should now be possible.

ACKNOWLEDGMENT

We are thankful to Brian Kincaid for supplying the data shown in this paper and for helpful discussion.

APPENDIX

When a photon is absorbed by an atom, a core hole is created to which the other electrons in the atom will respond. In this Appendix we shall discuss the implications of the core hole relaxation processes for EXAFS. In particular we shall discuss two aspects of the problem: (i) the effect of shake-up and shake-off processes on the absolute

magnitude of EXAFS, and (ii) the proper potential that we should use for the calculation of the central-atom phase shift.

The problem of core relaxation and the associated shake-off and shake-up processes have been studied extensively in photoemission. A detailed analysis has been made by Meldner and Perez²⁹ for photoemission on Ne. The energy distribution of the photoelectron shows a main peak corresponding to leaving the atom in its completely relaxed ground state. The relative weight of that peak is 74%. At lower photoelectron energy there are shake-up peaks corresponding to leaving the Ne⁺ ion in an excited state. However, these peaks carry a combined weight of only about 6%. The rest of the weight is distributed in a broad continuum that extends from 40 to over 140 eV below the main peak. These are shake-off processes where an electron is ejected into the continuum. The physical picture is that the ejection of the photoelectron suddenly creates an additional potential to which the rest of the electrons have to adjust. The wave functions ψ_i of the atom then has components corresponding to excited states ϕ_m of the ions. If the potential change takes place in time τ , then the sudden approximation is valid provided that the wave function is not changed during τ , i.e.,

$$\epsilon_m - \epsilon_i \ll 1/\tau, \quad (\text{A1})$$

where ϵ_i and ϵ_m are the energy of the states ψ_i and ϕ_m . Within the sudden approximation the probability of finding an electron originally in state ψ_i to be in the state ϕ_m is given by

$$P_{im} = \int |\phi_m^* \psi_i d\tau|^2. \quad (\text{A2})$$

Calculations based on this formula have been carried out by Carlson and Krause³⁰ and are in excellent agreement with experiment. Carlson and Krause also examined the relation of the time scale τ to the transit time of the photoelectron out of the atom. They have performed experiments with a variety of x-ray sources, thereby varying the photoelectron velocity. They have found that the shake-off probability initially increases with increasing photoelectron energy and saturates for photoelectron energy greater than 150 eV. More recent work and references can be found in Schmidt *et al.*³¹

The above picture suggests that the main feature in the EXAFS spectrum arises only from the fraction of the electrons ejected at the main peak. Electrons ejected with shake-up give rise to EXAFS also, but these will be shifted downward in energy by an amount equal to the excitation energy of the ion which is typically 10 to 30 eV. The shake-up peaks for Ne have a combined strength of only 6%. Such a small shifted spectrum will be difficult to detect experimentally. The shake-off peak contains more weight but it is distributed over such a wide energy range (of order 100 eV) that any EXAFS feature will be smeared out. We conclude on the basis of these considerations that calculated EXAFS spectra should be multiplied by the relative weight in the main peak in photoemission for energy greater than 150 eV above threshold before comparison is made with experiment.

The next question is how this relative weight can be determined experimentally. To obtain this information from photoemission requires detailed analysis as performed by Meldner and Perez for neon. The weight of the shake-off peak is too broad to be measured directly and has been measured by detecting the distribution of the number of charges on the ions,^{30,31} making use of the fact that shake-off processes leave the ions in a multiply charged state. This method is limited to the rare gases and has been performed only for He, Ne, and Ar. Another method is to study electron emission in β decay. It has long been recognized that an analogous physical process operates for photoemission and β decay where the nuclear charge is suddenly increased by one.³⁰ Shake-off processes will leave the ions with a charge greater than or equal to two. Most of the shake-up processes will leave the ions with charge plus one, except the few processes which leave behind a deep vacancy so that further Auger processes are energetically possible. A measurement of the

fraction of ions with charge plus one thus provides information on the fractional weight of the main peak and the shake-up lines. Such data are available for Ne, Ar, Kr, and Xe.³² The fraction of plus one ion is 79.1, 82, 79.2, and 80%, respectively. This fraction is relatively insensitive to atomic number, at least for rare-gas atoms. From these numbers we subtract approximately 6% to account for the shake-up processes, a number obtained for neon. In the solid most of the shake-up peaks are replaced by collective plasmon processes and this estimate of 6% is of course only approximate. We thus conclude that the fractional weight of the main peak is approximately 74%. The calculated EXAFS spectra should be reduced by this amount for energy \approx 150 eV above threshold before comparison is made with experiment.

We next consider the problem of the proper choice of the potential for the central atom. This potential is a time-dependent one as the wave function evolves from a completely unrelaxed state immediately after the excitation (the sudden approximation) to the completely relaxed state a long time afterward. The relaxation rate of each level is roughly given by its binding energy. To compare with these rates we need the time scale at which the central-atom potential enters into the EXAFS formula. We shall argue that this time scale is given by the transit time for the photoelectron to travel to the neighbor and back to the central atom. To see this we review the derivation of the EXAFS formula from the point of view of angular resolved photoemission.⁷ The probability of emission into a given direction \hat{k} is given by

$$P_1(\hat{k}) = |A_1(\hat{k})|^2, \quad (\text{A3})$$

where

$$A_1(\hat{k}) = \hat{e} \cdot \hat{k} + \frac{\hat{e} \cdot \hat{r}_1 e^{ikr_1(1-\cos\theta)} f(\theta)}{r_1}. \quad (\text{A4})$$

This equation describes the interference of the direct beam with the beam that is first directed toward the neighbor located at \vec{r}_1 and then scattered in the \hat{k} direction, the angle θ being that between \hat{k} and \hat{r}_1 . It can be shown⁷ that integration of $P_1(\hat{k})$ over all solid angles gives the EXAFS formula with the exception that the central atom term $e^{i2\phi_1}$ is missing. This is because the direct beam and the scattered beam are phase shifted by the same amount and the central atom phase shift must *cancel* to this order of approximation. It turns out that it is necessary to include the second-order process whereby the electron is backscattered by the neighbor at \vec{r}_1 toward the origin and is then scattered into the \hat{k} direction by the central atom

$$A_2(k) = \frac{\hat{\epsilon} \cdot \hat{r}_1 e^{2ikr_1} f(\pi) f'(\pi - \theta)}{r_1^2}. \quad (\text{A5})$$

It can be shown⁷ that the integration of this term over all \hat{k} supplies precisely the missing central-atom phase-shift term in the EXAFS formula. Thus even though the photoelectron eventually propagates to infinity, it is physically correct to think of it as going out to the neighbor and is scattered back to the origin as far as the $e^{i2\theta_1}$ term is concerned. Thus to evaluate this term we should use the central-atom potential at a time scale equal to the transit time

$$\tau^{-1} \approx v/2r_1 = k/2mr_1, \quad (\text{A6})$$

where v is the photoelectron velocity. In atomic units, $r \approx 4$ a.u. and for $k \approx 8$ a.u. we have $\tau^{-1} = 1$ a.u. or 27.2 eV. Thus it is safe to assume that all

the states bound more deeply than this energy have relaxed. The proper treatment of the valence electrons and the conduction-electron screening in the case of metals is more problematic. However, we shall argue that the errors made are of the same order as the change in the potential due to the chemical environment and we shall roughly account for all these effects by allowing E_0 to be an adjustable parameter.

Finally we point out that it is easy to construct a potential appropriate to a completely relaxed state in the presence of a core hole. We simply use the wave function for the next atom in the periodic table and remove one valence electron. The Coulomb potential due to the extra nuclear charge is canceled by one of the two 1s electrons so that the potential seen by the other electrons is the same as that in the presence of a core hole.

¹See review by L. V. Azaroff, *Rev. Mod. Phys.* **35**, 1012 (1963).

²D. E. Sayers, E. A. Stern, and F. W. Lytle, *Phys. Rev. Lett.* **27**, 1204 (1971); *Phys. Rev. B* **11**, 4836 (1975) and references therein.

³See for instance, B. M. Kincaid, P. Eisenberger, K. O. Hodgson, and S. Doniach, *Proc. Nat. Acad. Sci. (USA)* **72**, 2340 (1975).

⁴P. Eisenberger and B. M. Kincaid, *Chem. Phys. Lett.* **36**, 134 (1975).

⁵D. E. Sayers, E. A. Stern, and F. W. Lytle, *Phys. Rev. Lett.* **35**, 584 (1975).

⁶F. W. Lytle, D. E. Sayers, and E. B. Moore, Jr., *Appl. Phys. Lett.* **24**, 45 (1974).

⁷P. A. Lee, *Phys. Rev. B* **13**, 5261 (1976).

⁸B. M. Kincaid and P. Eisenberger, *Phys. Rev. Lett.* **34**, 1361 (1975).

⁹P. A. Lee and J. B. Pendry, *Phys. Rev. B* **11**, 2795 (1975).

¹⁰C. A. Ashley and S. Doniach, *Phys. Rev. B* **11**, 1279 (1975).

¹¹P. H. Citrin, P. Eisenberger, and B. M. Kincaid, *Phys. Rev. Lett.* **36**, 1346 (1976).

¹²G. Beni, P. A. Lee, and P. M. Platzman, *Phys. Rev. B* **13**, 5170 (1976).

¹³F. Bloch, *Z. Phys.* **81**, 363 (1933); H. Jensen, *ibid.* **106**, 620 (1937); P. Gombas, *ibid.* **121**, 523 (1943).

¹⁴W. Brandt and S. Lundqvist, *Phys. Rev.* **139**, A612 (1965); W. Brandt, L. Eder, and S. Lundqvist, *J. Quant. Spectrosc. Radiat. Transf.* **7**, 185 (1967).

¹⁵L. J. Sham and W. Kohn, *Phys. Rev.* **145**, 561 (1966).

¹⁶P. C. Hohenberg and W. Kohn, *Phys. Rev.* **136**, B864 (1964).

¹⁷S. K. Ma and K. A. Brueckner, *Phys. Rev.* **165**, 18

(1968).

¹⁸B. Y. Tong and L. J. Sham, *Phys. Rev.* **144**, 1 (1966).

¹⁹L. Hedin and S. Lundqvist, *Solid State Phys.* **23**, 1 (1969).

²⁰B. I. Lundqvist, *Phys. Kondens. Mater.* **6**, 206 (1967).

²¹D. R. Penn, *Phys. Rev. B* **12**, 5248 (1976).

²²E. Clementi and C. Roetti, *Atomic Data Nucl. Data Tables* **14**, 177 (1974).

²³Y. Marino, Y. Nakamura, and T. Iijima, *J. Chem. Phys.* **32**, 643 (1960).

²⁴D. E. Sayers (unpublished).

²⁵L. F. Mattheiss, *Phys. Rev.* **133**, A1399 (1964).

²⁶J. E. Demuth, P. M. Marcus, and D. W. Jepsen, *Phys. Rev. B* **11**, 1460 (1975).

²⁷E. C. Snow and J. T. Waber, *Phys. Rev.* **157**, 570 (1967).

²⁸For the case of copper it might be questioned whether the screening of the central ion by conduction electrons should be included. We have calculated θ_1' using a neutral $Z+1$ atom. The difference with the unscreened calculation is 0.15 and 0.4 radians at $k=8$ and 2, respectively. As discussed earlier this can be compensated for by a charge in E_0 and we find that the predicted nearest neighbor distance using these two sets of phase shifts differ only by 0.003 Å.

²⁹H. W. Meldner and J. D. Perez, *Phys. Rev. A* **4**, 1388 (1971).

³⁰T. A. Carlson and M. V. Krause, *Phys. Rev.* **140**, A1057 (1965).

³¹V. Schmidt, N. Sandner, H. Kuntzemüller, P. Dhez, F. Willeumier, and E. Kallne, *Phys. Rev. A* **13**, 1748 (1976).

³²T. A. Carlson, *Phys. Rev.* **131**, 676 (1963).